Comparison between grid side and inverter side current control for parallel interleaved grid connected converters

L. Bede, G. Gohil, T. Kerekes, M. Ciobotaru, R. Teodorescu and V. G. Agelidis

- ***Published in:*** 17th European Conference on Power Electronics and Applications (EPE'15 ECCE-Europe), Geneva, 2015
- ***DOI:*** doi: 10.1109/EPE.2015.7311745
- ***Publication date:*** 2015
- ***Citation for published version:*** L. Bede, G. Gohil, T. Kerekes, M. Ciobotaru, R. Teodorescu and V. G. Agelidis, "Comparison between grid side and inverter side current control for parallel interleaved grid connected converters," 2015 17th European Conference on Power Electronics and Applications (EPE'15 ECCE-Europe), Geneva, 2015, pp. 1-10.

Comparison between grid side and inverter side current control for parallel interleaved grid connected converters

Lorand Bede[1], Ghanshyamsinh Gohil[1], Tamas Kerekes[1], Mihai Ciobotaru[2], Remus Teodorescu[1], Vassilios G Agelidis[2]

Dept. of Energy Technology[1],
Aalborg University
Aalborg, Denmark
URL: www.iepe.et.aau.dk

School of Electrical Engineering[2],
University of New South Wales
Sydney, Australia
URL: http://www.unsw.edu.au/

Tel.: (+45) 2029 4814
E-Mail: lbe@et.aau.dk

Acknowledgements

The authors would like to thank the Intelligent Efficient Power Electronics (IEPE) program for supporting the related research.

Keywords

Interleaved converters, Voltage Source Converter (VSC), Converter control, Renewable energy systems

Abstract

To meet the ever stringent grid codes, the high power converter systems have multiple converters connected in parallel and require high order filters due to their limited switching capability. Controlling the grid current and, at the same time, ensuring equal current sharing is a challenge that these converters have to face. There are two main methods on how to control the output current of the converter system: either by directly controlling the total grid current and applying the same gate signals for all parallel converters, or by controlling the individual converters' currents. Using simulation and experimental results, this paper presents the advantages and disadvantages of both control methods when applied on a converter system consisting of two parallel interleaved converters connected to the electricity grid through a high order filter. For a better comparison, a controller design for both methods is also included.

Introduction

The penetration of wind power in utility grid networks has increased during the last decade [1]. To ensure a stable operation, more and more stringent grid codes are put into practice. One of the most stringent standards for the wind turbines is the German BDEW standard. This standard specifies the harmonic levels up to the 180^{th} harmonic, with special emphasis on some low order harmonics [2]. In order to meet these grid codes, the energy has to be processed by a Wind Energy Conversion System (WECS), which often employees a full scale converter [3]. The most commonly used converter is the Voltage Source Converter (VSC) [4].The power level capability of the VSCs is limited. To increase the power level of these converter systems, several similar converters have to be connected in parallel [5]. Moreover, the switching capability of the high power devices is rather low and high order filters are required to comply with the standard requirements. A trap filter is used in [6] to eliminate the switching harmonics from the grid current. The use of a trap filter combined with the grid side and converter side inductors can offer the required filtering, with reasonable size, to meet the BDEW standard.

The carriers of the parallel connected VSCs can be interleaved to reduce the filtering requirement and decrease the stress on the dc-link capacitor [7]. On the other hand, interleaving the carriers of the VSCs will lead to a high frequency circulating current to flow between the two VSCs[8]. This is caused by the phase shift between the pole voltages of the VSCs (measured with respect of the *O* point of the dc-link). The circulating current causes additional losses in the system and it should be minimized as much as possible. Several solutions have been proposed and used in the technical literature to suppress the circulating current. An isolation transformer is used at the output of every parallel converter in [9]. While, in [8] the authors use a common mode (CM) inductor, which is placed at the output of each parallel converter. Authors in [10-13] use a coupled inductor (CI) based solution, which is placed between the same phases of separate VSCs. The CI based solution is preferred in this paper. The drawback of this solution is that equal current sharing has to be ensured since unequal current sharing causes a low frequency circulating current to flow between the parallel converters.

Failing to comply with this might saturate the CI [11]. The unequal current sharing can be caused by multiple sources such as mismatches between the converter parameters (i.e. parasitic impedances, mismatches due to manufacturing) and because of differences in gate signals applied to the VSCs. The reference voltage waveforms of the converters are synthesized by using Pulse Width Modulated (PWM) signals. Authors in [14] investigated the effect of the different PWM schemes on the CI, regarding maximum flux density and core losses. It has been found out that the maximum core losses will occur if the DPWM1 method is used. In [15] a modified discontinuous PWM method is presented, which helps in reducing the size of the CI. On the other hand, the usage of DPWM1 results in the smallest switching losses for grid connected applications [16]. In this article for modulation the DPWM1 strategy is used, because of its' low switching losses.

Furthermore, the grid operator can specify the amount of the active and reactive power requirements for the WECS. In order to comply with these requirements, a grid current controller is needed [17]. Considering the topology presented in

Fig. 1 where two VSCs are connected in parallel, there are two possibilities on how to control the grid current. In the first case the feedback signal can be the grid current itself ($I_{x,g}$, where x represents the individual phase and x=[A;B;C]) and the controller calculates the duty cycles and applies them to both of the VSCs. The other method is to use the converter current as a feedback ($I_{x,1}$, $I_{x,2}$), and by doing this, individual current control is achieved and the grid current will be the sum of these two currents minus the current which flows through the trap branch. Both of these methods have their advantages and disadvantages with respect to performance, stability and implementation. From the grid point of view, the driving factor is the quality and power factor of the grid current. However, from converter point of view, an additional driving factor is to have small filters and to ensure a stable operation.

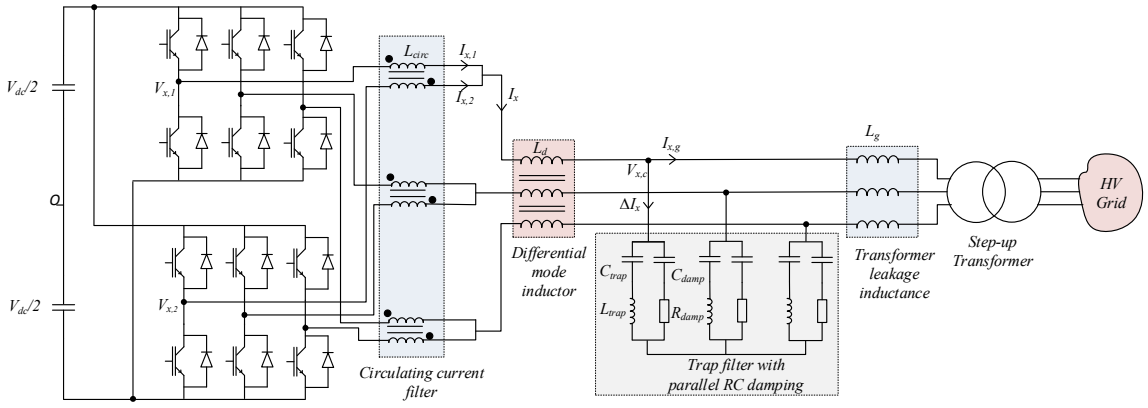

Fig. 1 Two parallel converters with trap filter connected to grid

This article presents a comparison between the converter current controller and the grid current controller, when a high order filter with passive damping is used. During the comparison the advantages and disadvantages of both of the solutions are presented through simulation and experimental results. The main focus is on current sharing performance of the two methods and their behaviour during steady state and transient operations. Furthermore, the transfer functions of both of the systems are presented, and a current controller is also designed for both of the cases. The results are illustrated on a simulation model and on an 11 kVA experimental test setup.

The article is structured as follows: The second section describes the system under test. The controller design and structure is presented in the third section. Then, the behaviour comparison between the investigated controllers under different conditions is presented. The experimental results followed by the conclusions are presented last.

System description

In Fig. 1, the schematic of the grid connected part of the WECS is depicted. The system contains two parallel connected VSCs, three CIs which are used as the circulating current filters (L_{circ}), a differential mode filter (L_d), a trap filter with a parallel RC damping and a step-up transformer. The transformer is needed in order to be able to connect to the medium voltage network. Furthermore, in Fig. 1, V_{dc} is the dc-link voltage, $I_{x,1}$ is the output current of VSC1, $V_{x,c}$ is the voltage

measured at the trap plus damping branch, C_{trap} is the capacitor of the trap filter, L_{trap} is the inductance of the trap filter, C_{damp} is damping capacitor, R_{damp} is the damping resistor. The switch current can be given as:

$$\begin{aligned} I_{x,1} &= I_{x1} + I_{x,c} \\ I_{x,2} &= I_{x2} - I_{x,c} \end{aligned} \tag{1}$$

where, I_x is the sum of the currents of the individual VSCs (I_{x1} and I_{x2}). The circulating current can be expressed from eq. (1)

$$I_{x,c} = \frac{I_{x,1} - I_{x,2}}{2} \tag{2}$$

If there are no control and hardware asymmetries between the VSCs, the current is shared equally between them (I_{x1}=I_{x2}). While, the total current can be written as

$$I_x = I_{x1} + I_{x2} \tag{3}$$

Thus, the grid current can be expressed as

$$I_{x,g} = I_x - \Delta I_x \tag{4}$$

where, ΔI_x is the current flowing into the trap branch.

By interleaving the carriers of the VSCs, the first order switching harmonic will not be present in the sum of the phase current (I_x), if an interleaving angle of 180^o is used. Furthermore, this interleaving angle has been chosen due to its optimal harmonic performance at high modulation indices [7, 18-20]. Since the first order switching harmonic is eliminated, the predominant current ripple in the total current will have a frequency twice the switching frequency (f_{sw}) [18]. To eliminate this harmonic content from the grid current ($I_{x,g}$), a trap filter is connected in parallel and its resonant frequency is tuned for twice the switching frequency.

For a better understanding and for modelling purposes, the single phase simplified scheme of the filter is presented by Fig. 2. This figure contains the converter and grid side inductors (L_d and L_g), the parallel trap branch with the parasitic resistance of the filter (C_{trap}, L_{trap} and R_{trap}), and the parallel passive RC damping branch (C_{damp}, R_{damp}). The resultant pole voltage ($V_{PWMx,avg}$) is the average of the individual pole voltages, which is given by

$$V_{PWMx,avg} = \frac{V_{x1O} + V_{x2O}}{2} \tag{5}$$

where, V_{x1O}, V_{x2O} is the pole voltage of VSC1 and VSC2, respectively and $V_{x,g}$ is the grid voltage.

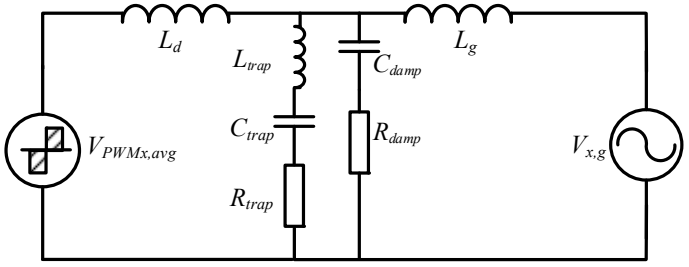

Fig. 2 Trap filter with parallel RC damping

Current controller design

Depending on the feedback variable, grid current or converter current, the model of the plant is different. In this section the transfer functions are presented for both cases. Moreover, the controller design is also shown for the above mentioned feedbacks.

The scheme of the control system is depicted by Fig. 3. The plant transfer function is $G_f(s)$, the delay introduced by the converter and the controller is represented by $G_d(s)$, and V_g is the feed forward term of the grid voltage, and I is the current feedback value. The current controller used for this analyses is the Proportional-Integral (PI) controller. Since, the PI controller has better performance for dc values than for ac values [17], the inputs and the outputs for the controller are obtained by using the synchronous reference frame.

The transfer function of the PI controller is represented by

$$G_{pi}(s) = K_p + \frac{K_i}{s} \tag{6}$$

where, K_p is the proportional gain, while K_i is the integral gain of the controller.

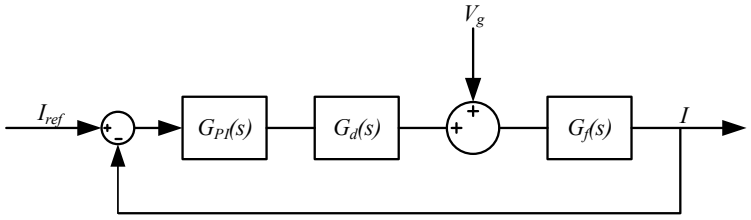

Fig. 3 Grid current controller including the grid voltage feed forward and delay introduced by the converter

As stated previously, the plant transfer function $G_f(s)$ depends on the feedback signal used. In this paper, two different feedback signals are considered: the first one is when the grid current is used as a feedback signal ($I_{x,g}$); and the second one is when the feedback signal is the converter side current i.e. $I_{x,1}$.

The transfer function of the converter ($G_d(s)$) is

$$G_d(s) = \frac{1}{1.5t_d s + 1} \tag{7}$$

where, t_d is $(1/2)fsw$.

Using the root locus theory, the parameters of the PI controller are obtained from the discrete time domain analysis. To obtain the discrete transfer functions, the continuous transfer functions were discretised using the Tustin method. For a fair comparison for both cases, the controllers were chosen to have a damping factor of 0.7. The values of the parameters used for the simulation and experimental results are given in Table I.

Table I System Parameters

Parameters	Value
Power	11 kVA
Switching frequency	2.55 kHz
DC-link voltage	650 V
Filter inductance L_d	2.2 mH
Grid side inductance L_g	3.6 mH
Trap capacitor C_{trap}	4.4 µF
Damping capacitor C_{damp}	2.2 µF
Trap inductor L_{trap}	232 µH
Damping resistor R_{damp}	30 Ω
Trap branch resistance R_{trap}	1 Ω
Modulation Method	DPWM1

Grid current controller-grid current feedback

When the grid current ($I_{x,g}$) is used as a feedback signal the transfer function of the plant is described by (8).

$$\frac{I_{x,g}(s)}{V_{PWMx,avg}(s)} = \frac{s^3 L_{trap}C_{trap}C_{damp}R_{damp} + s^2 C_{trap}\left(C_{damp}R_{trap}R_{damp} + L_{trap}\right) + s\left(C_{trap}R_{trap} + C_{damp}R_{damp}\right) + 1}{\left(\begin{array}{c} s^5 L_d L_g L_{trap} C_{damp} + s^4 C_{trap}C_{damp}\left(L_g L_{trap}R_{damp} + L_d L_{trap}R_{damp} + L_d L_g R_{trap} + L_d L_g R_{damp}\right) + \\ s^3\left[L_d L_g\left(C_{trap} + C_{damp}\right) + L_{trap}C_{trap}\left(L_d + L_g\right) + C_{trap}C_{damp}R_{damp}\left(L_g + L_d R_{trap}\right)\right] + \\ s^2\left[\left(L_g + L_d\right)\left(C_{trap}R_{trap} + C_{damp}R_{damp}\right)\right] + s\left(L_d + L_g\right) \end{array}\right)} \tag{8}$$

To achieve the desired damping factor (0.7) for the system with the grid current feedback K_p parameter is 9 and K_i is 3400.

In Fig. 4, the root loci of the transfer function defined in (8) is depicted, while in Fig. 5 the Bode plot of the system, where the grid current is used as an output, is presented. The value for the K_P is read from the root locus plot, while the value of the K_i is chosen to be the value of the dominant pole (closest to the origin) of the transfer function in (8). The Bode plot shows the frequency response of the system, with and without the controller.

Grid current controller-converter side current feedback

The same procedure has been repeated for the system when the output of the transfer function is the converter current. In this case it has been found out that the K_P value is 11.5 while K_i is 3400, for the same design criteria. It can be noted that in this case the parameters are the same as in Table I, the only difference is that the value of L_d is twice compared to the previous case. This is due to the fact that the plant seen by the controller contains two filter inductances connected in parallel and its resultant value is L_d.

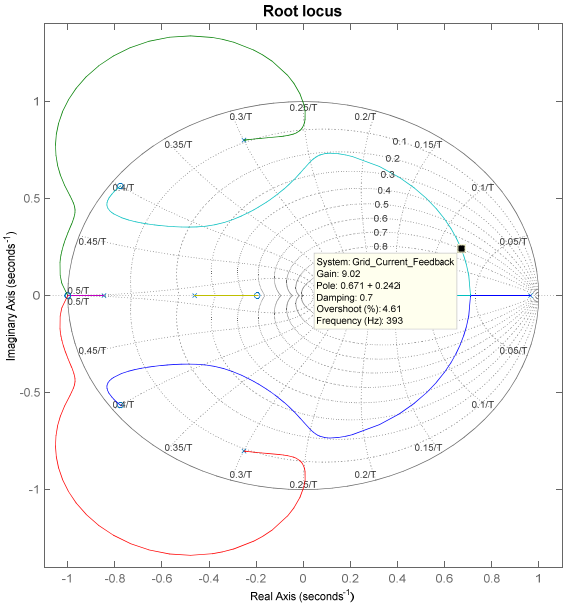

Fig. 4 Root locus plot of the transfer function where the output is the grid current

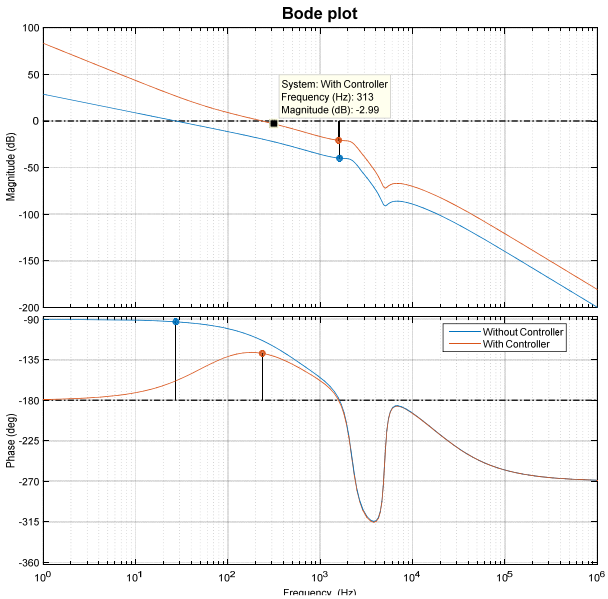

Fig. 5 Bode plot of the system of the transfer function where the output is the grid current; without (blue line) and with (red line) controller

$$\frac{I_{x,1}(s)}{V_{PWMx,avg}(s)} = \frac{\begin{pmatrix} s^4 L_g L_{trap} C_{trap} C_{damp} + s^3 \left(L_{trap} C_{trap} C_{damp} R_{damp} + L_g C_{trap} C_{damp} R_{trap} + L_g C_{trap} C_{damp} R_{damp} \right) + \\ s^2 L_g \left(L_g C_{trap} + L_g C_{damp} + C_{trap} C_{damp} R_{trap} R_{damp} + L_{trap} C_{trap} \right) + s\left(C_{trap} R_{trap} + C_{damp} R_{damp} \right) + 1 \end{pmatrix}}{\begin{pmatrix} s^5 L_d L_g L_{trap} C_{trap} C_{damp} + s^4 C_{trap} C_{damp} \left\{ L_g L_{trap} R_{damp} + L_d \left[L_{trap} R_{damp} + L_g (\mathrm{R_{trap}} + \mathrm{R_{damp}}) \right] \right\} + \\ s^3 \left\{ L_g C_{trap} \left(C_{damp} R_{trap} R_{damp} + L_{trap} \right) + L_d \left[C_{trap} \left(C_{damp} R_{trap} R_{damp} + L_{trap} \right) + L_g \left(C_{trap} + C_{damp} \right) \right] \right\} + \\ s^2 \left(C_{trap} R_{trap} + C_{damp} R_{damp} \right) \left(L_d + L_g \right) + s\left(L_d + L_g \right) \end{pmatrix}} \quad (9)$$

In the Fig. 6, the root loci of the transfer function defined in (9) is depicted, and in Fig. 7 the Bode plot of the same transfer function is presented.

Comparison of the system with the grid current feedback and the converter current feedback

When comparing the Bode plots for the two cases (Fig. 4 and Fig. 6), it can be observed that both of the systems are stable, and they have similar phase margins. Furthermore, the bandwidth of the controllers are close to each other. For the grid current feedback is 313 Hz and for the converter current feedback is 277 Hz.

However, when the root loci of the two transfer functions are compared (Fig. 5 and Fig. 7), it can be noticed that when the converter current is used as a feedback, the poles will remain inside the unity circle. While, when the grid current is used, the poles will move outside of the unity circle if the gain is about a certain value.

The simulation results were conducted using MATLAB/Simulink and PLECS software environment. During the simulation study, at 0.06 s there is a step change in the I_d reference grid current from 20% to 100%. For the grid current feedback case, the step was applied for the grid current from 20% to 100%, while for the other case, the reference change was applied for the converter current. Because of the existence of the trap branch

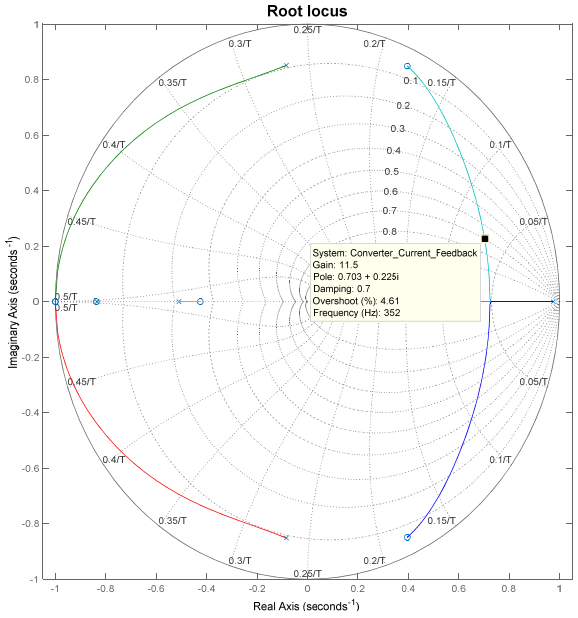

Fig. 6 Root locus plot of the transfer function in (8)

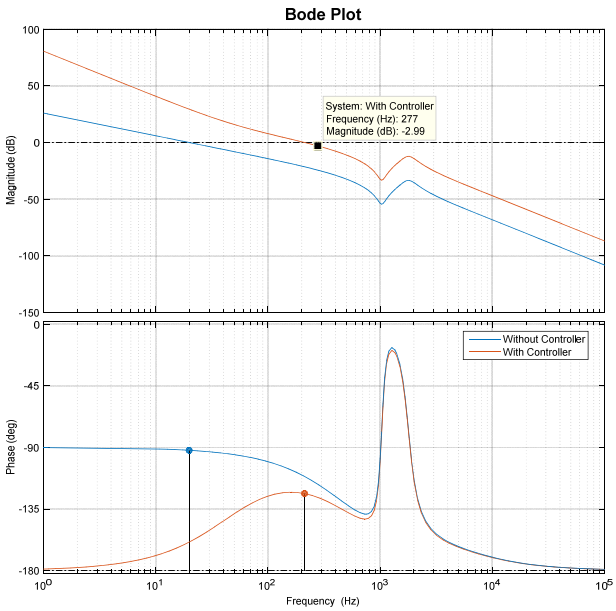

Fig. 7 Bode plot of the system without (blue line) and with (red line) controller

and the passive damping, in the case of converter current control the power factor of the grid current will not be 1. For both of the feedback cases the following quantities are shown: (a) current of phase A for VSC1 and the same current for VSC2 (b); the circulating current between the converters (c); the sum of these two currents in (d); while in (e) the normalized grid current and grid voltage are presented. Although the behaviour of the system for both of the cases is similar, there is a difference in the circulating current. When the grid current is used as a feedback, the circulating current only has high frequency components. However, for the case when the converter currents are used as feedback, the circulating current has a 50Hz component. This is due to the fact that in the case of converter current control, the controllers will have different outputs because the controllers work against each other. While in the case of the grid current feedback, the same reference signals are applied to both of the converters. The results are presented for the grid current feedback in Fig. 9, while Fig. 8 shows the results for the converter current feedback.

For a better comparison of the controllers' performance, I_d and I_q currents are presented in Fig. 10. As previously mentioned, there was a step change applied for the current references at 0.06s. The I_q current for the case of the grid current feedback is 0 whilst the I_q current for the converter current feedback has an offset. This is expected since, there is no compensation for the current taken by the trap branch and the passive damping. The step change is only applied for the I_d current, but because of the lack of the cross coupling term it has an effect also on the I_q current. However, the authors consider that the effect is small and there is no need for adding the cross coupling terms.

Experimental Results

In order to test the performance of the two different controllers, an experimental setup consisting of two VSCs connected in parallel has been built. The controller was implemented using the Texas Instrument TMS320F28346 microcontroller unit. The parameters of the system were identical with the ones used for simulation. To avoid grid harmonics, an MX30 grid emulator from California Instruments has been used. During the experimental tests, steady state and transient operation was observed for both of the feedback cases. To test the performance of the controller during transient operation, a load step was introduced from 20% to 100% load. When comparing the converter currents during steady state operation for the grid current feedback (Fig. 11) with the converter current feedback (Fig. 15) case, it has to be noted that the RMS values of the converter currents (I_{A1} and I_{A2}) are not equal for both situations. Because the circulating current is the difference

of these currents, for the case of the converter current feedback the circulating current will have a 50Hz component. This can be explained by the difference between the reference signals applied to the VSCs by the individual controllers.

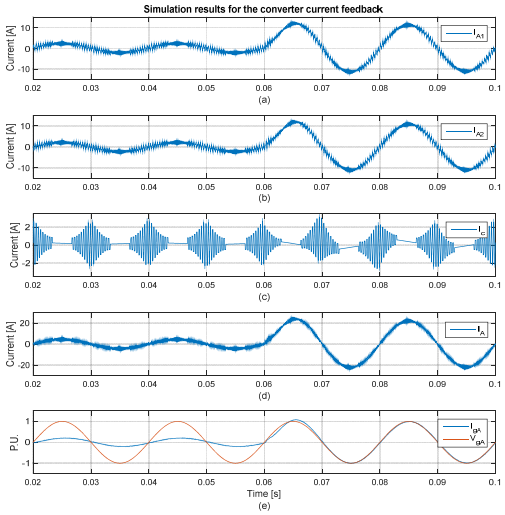

Fig. 8 Simulation results - Converter current feedback: for a step change from 20% to 100% load; (a) - phase A current VSC1; (b) - phase A current VSC2; (c) - Circulating current (I_c) between Phase A VSC1 and phase A VSC2; (d) – Total Current ($I_{x,A}$); (e) – normalized grid current(I_{gA}) and voltage (V_{gA})

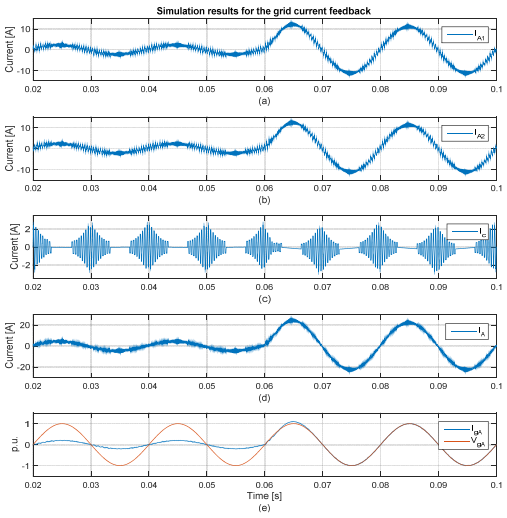

Fig. 9 Simulation results - Grid current feedback: for a step change from 20% to 100% load; (a) - phase A current VSC1; (b) - phase A current VSC2; (c) - Circulating current (I_c) between Phase A VSC1 and Phase A VSC2; (d) – Total Current ($I_{x,A}$); (e) – normalized grid current(I_{gA}) and voltage (V_{gA})

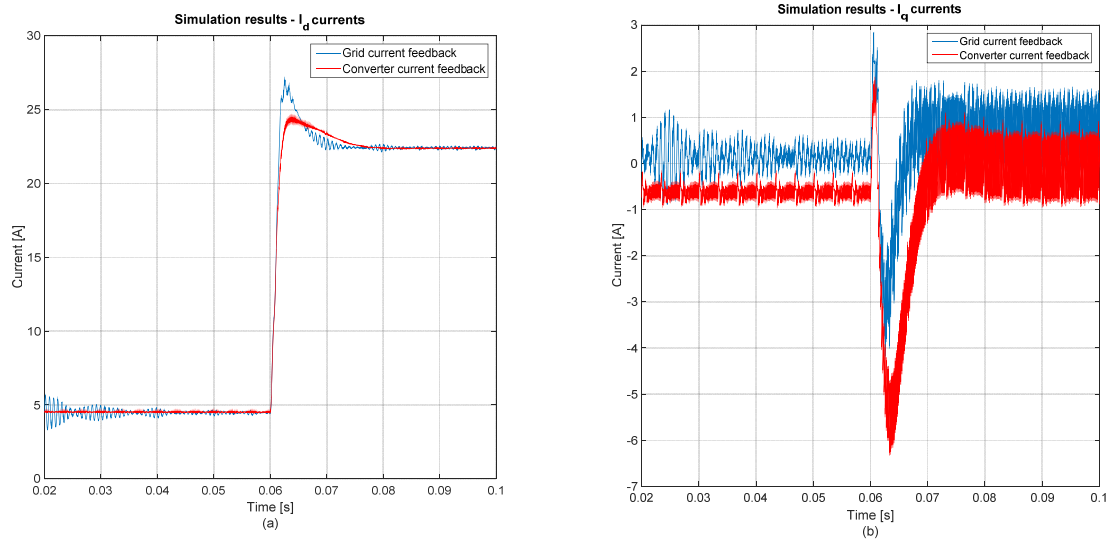

Fig. 10 Simulation results: I_d (a) and I_q (b) components of the grid current for a step change in the load from 20%

The grid current and voltage is presented for the steady state (Fig. 13 for grid current feedback and Fig. 15 for converter current feedback, respectively). The transient response is captured in Fig. 12 for the grid current feedback and Fig. 16 for the converter current feedback, respectively. When the grid current is used as a feedback, the circulating current remains the same before and after the step change has been applied. However, in the other case the 50Hz component of the circulating current is higher after the reference has been changed. Meaning that the difference between the controllers output is higher for higher current references. The performance of the individual currents is similar for both cases. The grid current in the case of the grid current feedback (Fig. 14) has a slightly bigger overshoot than it is for the converter current feedback (Fig. 18). All of the experimental results prove that the findings in the simulation are valid.

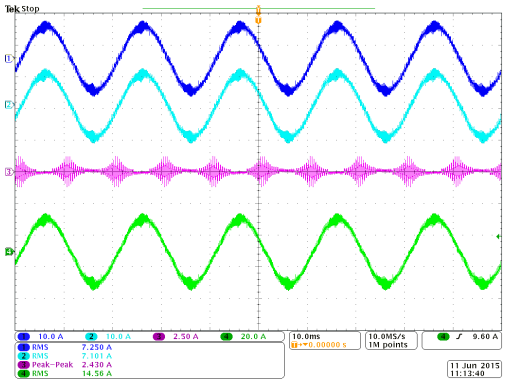

Fig. 11 Grid current feedback: Experimental results for nominal load; Ch1 (*blue*) -phase A current VSC1; Ch2 (*light blue*) - phase A current VSC2; Ch3 (*magenta*) - Circulating current (I_c) between Phase A VSC1 and Phase A VSC2; Ch4 (*green*) – Total Current ($I_{x,A}$)

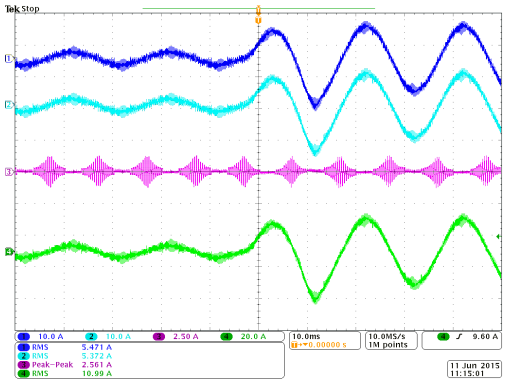

Fig. 12 Grid current feedback: Experimental results for a step change from 20% to 100% load; Ch1 (*blue*) -phase A current VSC1; Ch2 (*light blue*) - phase A current VSC2; Ch3 (*magenta*) - Circulating current (I_c) between Phase A VSC1 and Phase A VSC2; Ch4 (*green*) – Total Current ($I_{x,A}$)

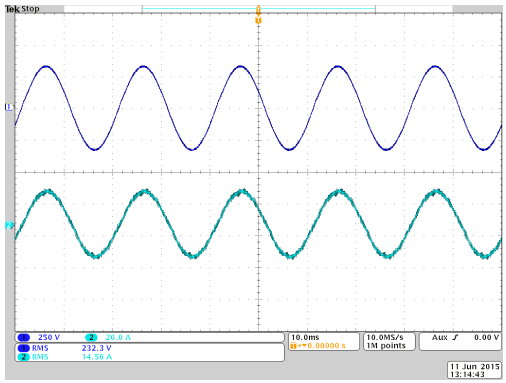

Fig. 13 Grid current feedback: Experimental results for nominal load; Ch1 (*blue*) -phase A grid voltage; Ch2 (*light blue*) - phase A grid current ($I_{g,A}$);

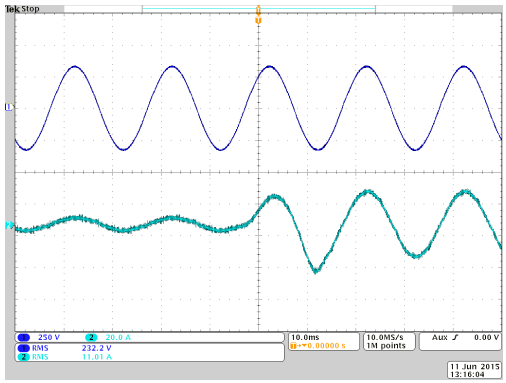

Fig. 14 Grid current feedback: Experimental results for a step change from 20% to 100% load; Ch1 (*blue*) -phase A grid voltage; Ch2 (*light blue*) - phase A grid current ($I_{g,A}$);

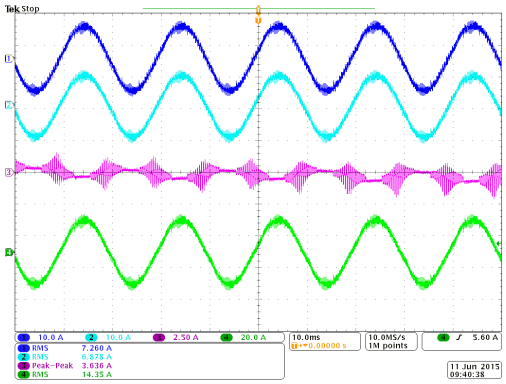

Fig. 15 Converter current feedback: Experimental results for nominal load; Ch1 (*blue*) -phase A current VSC1; Ch2 (*light blue*) - phase A current VSC2; Ch3 (*magenta*) - Circulating current (I_c) between Phase A VSC1 and Phase A VSC2; Ch4 (*green*) – Total Current ($I_{x,A}$)

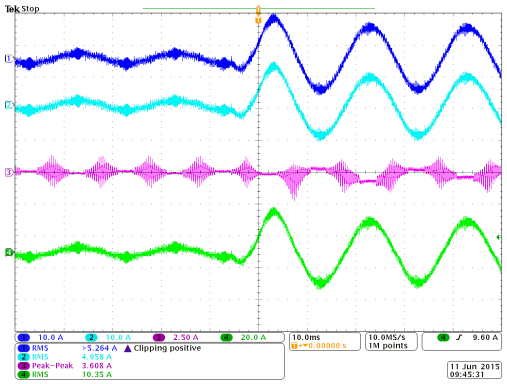

Fig. 16 Converter current feedback: Experimental results for a step change from 20% to 100% load; Ch1 (*blue*) - phase A current VSC1; Ch2 (*light blue*) - phase A current VSC2; Ch3 (*magenta*) - Circulating current (I_c) between Phase A VSC1 and Phase A VSC2; Ch4 (*green*) – Total Current ($I_{x,A}$)

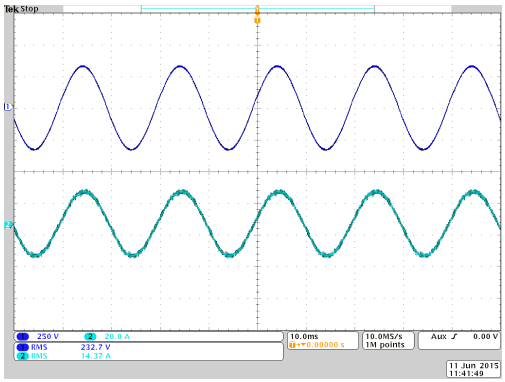

Fig. 17 Converter current feedback: Experimental results for nominal load; Ch1 (*blue*) -phase A grid voltage; Ch2 (*light blue*) - phase A grid current ($I_{g,A}$);

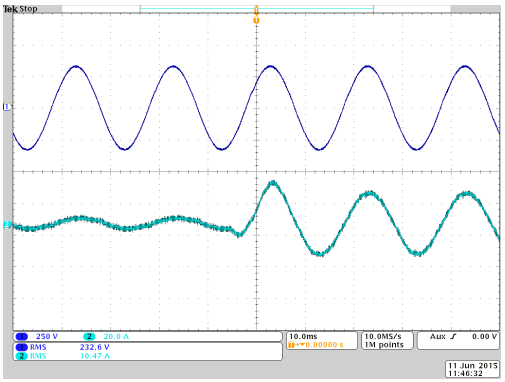

Fig. 18 Converter current feedback: Experimental results for a step change from 20% to 100% load; Ch1 (*blue*) - phase A grid voltage; Ch2 (*light blue*) - phase A grid current ($I_{g,A}$);

Conclusion

In this paper the focus was on differences between the current controllers used to control a high order filter interfaced grid connected converter system. It can be concluded that the performance of the current controllers are different even though the design criteria for the controller design was the same. When the same control signals are applied for both of the converters, the current between the VSCs is shared equally if there is no difference in the system parameters. Another advantage of this solution is that it is enough to measure only the grid current, there is no need to measure the individual VSC currents. However, if there is mismatch in the parameters between the VSCs, a low order circulating current will appear between the VSCs which has to be suppressed, this can only be done by introducing a circulating current controller. Moreover, the circulating current will required the individual VSC currents, hence additional sensors are required increasing the cost of the system.

On the other hand, if every VSC has its own current controller, there is no need for the grid current sensor. Because the individual current controllers are working against each other and because of the parameter mismatches between the VSCs there will be a low frequency circulating current, which has to be controlled. In this case there is no need for additional current sensors. However, because of the presence of a parallel trap filter and passive damping, the correct power factor of the power injected to the grid can only be ensured if there is a compensation for the reactive power consumption of the trap filter and passive damping. This can be done by either, measuring the current which is going to the parallel connected trap filter and passive damping, or by measuring the grid current or by knowing the parameters of the trap filter and the passive damping, one can estimate the reactive power flowing into it and can compensate for it.

Regarding the transient operation, it can be concluded that for the given design criteria (damping factor of 0.7) the grid current controller will have a little bit bigger bandwidth, however, the gain of the system in this case has to be carefully selected, since the system will become instable for a variety of gains. This problem is not present in the converter current feedback case, since from the root locus it can be seen that the poles of the system remain inside the unity circle.

References

[1] F. Blaabjerg, M. Liserre, and M. Ke, "Power Electronics Converters for Wind Turbine Systems," *Industry Applications, IEEE Transactions on,* vol. 48, pp. 708-719, 2012.

[2] A. A. Rockhill, M. Liserre, R. Teodorescu, and P. Rodriguez, "Grid-Filter Design for a Multimegawatt Medium-Voltage Voltage-Source Inverter," *Industrial Electronics, IEEE Transactions on,* vol. 58, pp. 1205-1217, 2011.

[3] C. Zhe, J. M. Guerrero, and F. Blaabjerg, "A Review of the State of the Art of Power Electronics for Wind Turbines," *Power Electronics, IEEE Transactions on,* vol. 24, pp. 1859-1875, 2009.

[4] F. Blaabjerg, M. Liserre, and K. Ma, "Power electronics converters for wind turbine systems," in *Energy Conversion Congress and Exposition (ECCE), 2011 IEEE*, 2011, pp. 281-290.

[5] R. Jones and P. Waite, "Optimised power converter for multi-MW direct drive permanent magnet wind turbines," in *Power Electronics and Applications (EPE 2011), Proceedings of the 2011-14th European Conference on*, 2011, pp. 1-10.

[6] G. Gohil, L. Bede, R. Teodorescu, T. Kerekes, and F. Blaabjerg, "Design of the trap filter for the high power converters with parallel interleaved VSCs," in *Industrial Electronics Society, IECON 2014 - 40th Annual Conference of the IEEE*, 2014, pp. 2030-2036.

[7] J. S. S. Prasad and G. Narayanan, "Minimization of Grid Current Distortion in Parallel-Connected Converters Through Carrier Interleaving," *Industrial Electronics, IEEE Transactions on,* vol. 61, pp. 76-91, 2014.

[8] L. Asiminoaei, E. Aeloiza, P. N. Enjeti, and F. Blaabjerg, "Shunt Active-Power-Filter Topology Based on Parallel Interleaved Inverters," *Industrial Electronics, IEEE Transactions on,* vol. 55, pp. 1175-1189, 2008.

[9] J. W. Dixon and B. T. Ooi, "Series and parallel operation of hysteresis current-controlled PWM rectifiers," *Industry Applications, IEEE Transactions on,* vol. 25, pp. 644-651, 1989.

[10] P. In Gyu and K. Seon Ik, "Modeling and analysis of multi-interphase transformers for connecting power converters in parallel," in *Power Electronics Specialists Conference, 1997. PESC '97 Record., 28th Annual IEEE*, 1997, pp. 1164-1170 vol.2.

[11] B. Cougo, G. Gateau, T. Meynard, M. Bobrowska-Rafal, and M. Cousineau, "PD Modulation Scheme for Three-Phase Parallel Multilevel Inverters," *Industrial Electronics, IEEE Transactions on,* vol. 59, pp. 690-700, 2012.

[12] F. Forest, E. Laboure, T. A. Meynard, and V. Smet, "Design and Comparison of Inductors and Intercell Transformers for Filtering of PWM Inverter Output," *Power Electronics, IEEE Transactions on,* vol. 24, pp. 812-821, 2009.

[13] B. Cougo, T. Meynard, and G. Gateau, "Parallel Three-Phase Inverters: Optimal PWM Method for Flux Reduction in Intercell Transformers," *Power Electronics, IEEE Transactions on,* vol. 26, pp. 2184-2191, 2011.

[14] G. Gohil, L. Bede, R. Maheshwari, R. Teodorescu, T. Kerekes, and F. Blaabjerg, "Parallel interleaved VSCs: Influence of the PWM scheme on the design of the coupled inductor," in *Industrial Electronics Society, IECON 2014 - 40th Annual Conference of the IEEE*, 2014, pp. 1693-1699.

[15] G. Gohil, R. Maheshwari, L. Bede, T. Kerekes, R. Teodorescu, M. Liserre*, et al.*, "Modified Discontinuous PWM for Size Reduction of the Circulating Current Filter in Parallel Interleaved Converters," *Power Electronics, IEEE Transactions on,* vol. 30, pp. 3457-3470, 2015.

[16] G. Gohil, L. Bede, R. Teodorescu, T. Kerekes, and F. Blaabjerg, "Line Filter Design of Parallel Interleaved VSCs for High Power Wind Energy Conversion System," *Power Electronics, IEEE Transactions on,* vol. PP, pp. 1-1, 2015.

[17] A. Timbus, M. Liserre, R. Teodorescu, P. Rodriguez, and F. Blaabjerg, "Evaluation of Current Controllers for Distributed Power Generation Systems," *Power Electronics, IEEE Transactions on,* vol. 24, pp. 654-664, 2009.

[18] S. K. T. Miller, T. Beechner, and S. Jian, "A Comprehensive Study of Harmonic Cancellation Effects in Interleaved Three-Phase VSCs," in *Power Electronics Specialists Conference, 2007. PESC 2007. IEEE*, 2007, pp. 29-35.

[19] Z. Di, F. Wang, R. Burgos, L. Rixin, and D. Boroyevich, "Impact of Interleaving on AC Passive Components of Paralleled Three-Phase Voltage-Source Converters," *Industry Applications, IEEE Transactions on,* vol. 46, pp. 1042-1054, 2010.

[20] M. A. Abusara and S. M. Sharkh, "Design and Control of a Grid-Connected Interleaved Inverter," *Power Electronics, IEEE Transactions on,* vol. 28, pp. 748-764, 2013.